

# Rate-Splitting Multiple Access for Overloaded Multi-group Multicast: A First Experimental Study

Xinze Lyu, *Student Member, IEEE*, Sundar Aditya, *Member, IEEE* and Bruno Clerckx, *Fellow, IEEE*

**Abstract**—Multi-group multicast (MGM) is an increasingly important form of multi-user wireless communications with several potential applications, such as video streaming, federated learning, safety-critical vehicular communications, etc. Rate-Splitting Multiple Access (RSMA) is a powerful interference management technique that can, in principle, achieve higher data rates and greater fairness for all types of multi-user wireless communications, including MGM. This paper presents the first-ever experimental evaluation of RSMA-based MGM, as well as the first-ever three-way comparison of RSMA-based, Space Division Multiple Access (SDMA)-based and Non-Orthogonal Multiple Access (NOMA)-based MGM. Using a measurement setup involving a two-antenna transmitter and two groups of two single-antenna users per group, we consider the problem of realizing throughput (max-min) fairness across groups for each of three multiple access schemes, over nine experimental cases in a line-of-sight environment capturing varying levels of pathloss difference and channel correlation across the groups. Over these cases, we observe that RSMA-based MGM achieves fairness at a higher throughput for each group than SDMA- and NOMA-based MGM. These findings validate RSMA-based MGM’s promised gains from the theoretical literature.

**Index Terms**—Rate-Splitting Multiple Access (RSMA), Multi-group multicast (MGM), RSMA prototyping, RSMA measurements.

## I. INTRODUCTION

Multi-group multicast (MGM) is a special case of multi-user wireless communications, wherein a multi-antenna transmitter (TX) jointly communicates with several *groups* of users simultaneously. The  $g$ -th group (integer  $g$ ) has  $N_g$  users, where  $N_g \geq 1$  in general, and each user within this group desires the same message from the TX. The special case of a single group corresponds to multicast/broadcast communications, whereas  $N_g = 1$  (for each  $g$ ) corresponds to unicast communications.

MGM is a key physical (PHY) layer enabler of several *group* applications, such as video streaming, push-to-talk group radio communications, location-based services, safety-critical vehicular communications, etc [1]. The importance of these applications in future wireless networks is driving ongoing standardization efforts on how best to support multicast/broadcast service (MBS) in future wireless standards, most notably in 3GPP (Third Generation Partnership Project) [2].

Analogous to unicast, MGM can be realized through linear precoding (beamforming) at the TX, but with two key differences that need to be factored into the precoder design:

- MGM involves the additional constraint that each user within a group must be able to decode its desired message. In general, a wide range of *spatial geometries* may be possible in terms of group composition, resulting in a great variety of channels experienced by users in a group. However, a special case of considerable practical interest is where users within a group are closely situated and experience *similar* channels, spanning a spectrum from similar channel strengths at one end, all the way to high spatial correlation/alignment at the other. This could arise in applications like gaming, video conferencing, vehicular swarms, etc. Hence, we focus on this special case in this paper.
- Additionally, in many MGM applications such as satellite communications [3] and Internet-of-Things (IoT) [4], the number of users is also likely to exceed the number of antennas at the TX. Hence, we further focus on such *overloaded* scenarios for which interference management is even more challenging, since the interference power at all users cannot be suppressed to arbitrarily low levels.

The above factors have given rise to the following precoder design approaches in the literature, motivated by well-known analogues for unicast:

- a) *SDMA-based MGM*: Most of the existing literature [5]–[14] on MGM focuses on this approach, which is an extension of Space Division Multiple Access (SDMA) for unicast. Thus, each group is treated as a super-user, resulting in one precoder per group, and the precoders are designed to suppress the power of the *inter-group* interference so that it can be treated as noise. While there are several well-motivated objectives for precoder design in MGM, arguably the most popular in the literature is (max-min) rate fairness across the different groups<sup>1</sup>. For SDMA-based MGM, this problem has been investigated analytically in many settings, namely [5], [6] (with a sum power constraint), [7] (with a per antenna power constraint), [8] (with low-complexity precoder design for large-scale transmit antennas) and [9] (for line-of-sight groups), [10] (for satellite communications), [13] (for cooperative integrated terrestrial-satellite communications). However, to the best of our knowledge, an experimental evaluation of SDMA-based MGM does not exist in the literature. The existing experimental studies

This work was supported in part by UKRI Impact Acceleration Account (IAA) grant EP/X52556X/1.

X. Lyu, S. Aditya and B. Clerckx are with the Dept. of Electrical and Electronic Eng., Imperial College London, London SW7 2AZ, U.K. (e-mail: {x.lyu21, s.aditya, b.clerckx}@imperial.ac.uk).

<sup>1</sup>Other objectives for MGM precoder design include (i) minimizing transmit power subject to minimum rate constraints at each group [9]–[11], (ii) maximizing sum rate under a per antenna power constraint [12], and (iii) extending zero-forcing and MMSE precoding for MGM [14].

have focused on implementing MGM at higher layers [15], [16], instead of the PHY layer.

- b) *NOMA-based MGM*: This approach is an extension of power domain Non-Orthogonal Multiple Access (NOMA), and is guided by the principle that decoding the interference rather than treating it as noise is more effective for overloaded scenarios, particularly for unicast [17]. Like above, this approach also yields one precoder per group, but for the two-group case, one of the groups employs successive interference cancellation (SIC) to decode and subtract the interference, just like the *stronger user* in unicast NOMA. Precoder optimization<sup>2</sup> for NOMA-based MGM was investigated in [21], [22] (objective: minimizing transmit power subject to minimum rate constraints at each group). However, even for the overloaded scenario, NOMA-based MGM exhibited significant gains over SDMA-based MGM only when there is considerable disparity in channel strength across the groups [22]. Moreover, for groups of closely-spaced users with large angular separation between groups, it is plausible that SDMA-based MGM may still be effective in suppressing inter-group interference by exploiting the spatial domain, even in overloaded scenarios. The potential underperformance of NOMA-based MGM relative to SDMA-based MGM in such scenarios, despite a higher receiver complexity, is due to the former's inability to exploit the multi-antenna multiplexing gain [23], [24]. For a clearer picture of the circumstances under which NOMA-based MGM is superior to SDMA-based MGM (in terms of realizing max-min rate fairness across groups, say), an experimental study of the two schemes over a variety of group spatial geometries is needed, something that is missing in the literature.
- c) *RSMA-based MGM*: Inspired by the superiority of Rate-Splitting Multiple Access (RSMA) over both SDMA and NOMA for unicast [25], [26], this approach bridges a) and b) above to address their limitations. Specifically, each group *partially* decodes the inter-group interference and *partially* treats it as noise [27]. All groups have the same signal processing complexity for retrieving their desired messages (one stage of SIC, regardless of the number of groups). Unlike a) and b), this approach yields one more precoder than the number of groups (details in Section II). Precoder optimization for RSMA-based MGM was investigated in [24], [28], [29] (objective: max-min rate fairness across groups), where it was demonstrated analytically that RSMA-based MGM achieved a higher minimum rate than the other two approaches. This was validated using link-level simulations in [30] (under perfect CSIT) and [29], [31], [32] (for satellite communications). However, for a clearer picture of the extent of such gains, an experimental comparison of the three MGM approaches over a variety of group spatial geometries is needed.

Indeed, it is surprising that an experimental evaluation of MGM for any of the above multiple access schemes is missing from the literature. In this paper, we address this gap by conducting the first-ever experimental comparison of the fairness performance of RSMA-, SDMA- and NOMA-based MGM. Our contributions are as follows:

- For two groups with two users per group, we formulate the practically relevant *MCS-limited* max-min throughput fairness problem for RSMA-based MGM. In the process, we explain how RSMA-based MGM has an advantage over SDMA- and NOMA-based MGM in terms of realizing max-min fairness through a flexible allocation of the common stream (Section II-B).
- Using our RSMA prototype (Section III), we empirically solve the above-defined MCS-limited max-min fairness problem through measurements. In our experiments (Section IV), we realize nine cases, with the intention of capturing a wide variety in terms of pathloss difference and spatial correlation between the two groups (subject to closely situated users in each group). Over these nine cases, we observe that RSMA-based MGM achieves fairness at a higher minimum throughput than SDMA- and NOMA-based MGM. This is consistent with theoretical predictions [24], [28], [30].

#### A. Notation

Column vectors are represented by lowercase bold letters (e.g.,  $\mathbf{h}$ ).  $|\cdot|$  denotes the magnitude of scalars and cardinality of sets.  $\mathbb{E}[\cdot]$ ,  $(\cdot)^H$ ,  $\|\cdot\|$ ,  $\cup$  and  $\emptyset$  denote the expectation operator, the Hermitian operator, the Euclidean norm, set union and the empty set, respectively.  $\mathcal{CN}(0, \sigma^2)$  denotes the circularly symmetric complex Gaussian distribution with zero mean and variance  $\sigma^2$ .

## II. SYSTEM MODEL

Without loss of generality, we consider MGM involving two groups, with each group comprising two single-antenna users (i.e.,  $N_1 = N_2 = 2$ ). Each user belongs to exactly one group, and we assume that the composition of the groups is known a priori to the TX. For brevity, let  $(u, g)$  denote user  $u$  in group  $g$ . All the users within a group desire the same message from the TX, which is communicated over two stages – in the first stage, the TX acquires channel state information (CSIT), which is used in the second stage to design the RSMA-based MGM precoders and transmit signal. The two stages are described in more detail next.

#### A. Stage 1: CSIT Acquisition

We consider data transmission using OFDM signals over  $N_c$  subcarriers. Let  $N_t$  denote the number of antenna elements at the TX, and let  $\mathbf{h}_{u,g}[k] \in \mathbb{C}^{N_t}$  denote the slowly varying, flat fading channel experienced by  $(u, g)$  over the  $k$ -th subcarrier ( $k = 0, \dots, N_c - 1$ ). Through orthogonal pilots transmitted by the TX,  $(u, g)$  obtains an estimate of  $\mathbf{h}_{u,g}[k]$ , denoted by

<sup>2</sup>Note: NOMA-based MGM has also been investigated for single-antenna systems [18] and multi-antenna systems without precoder optimization [19], [20].

$\hat{\mathbf{h}}_{u,g}[k]$ . To reduce CSI feedback overhead,  $(u, g)$  evaluates the *wideband CSI* by averaging  $\mathbf{h}_{u,g}[k]$  over the subcarriers, i.e.,

$$\hat{\mathbf{h}}_{u,g} := \frac{1}{N_c} \sum_{k=0}^{N_c-1} \hat{\mathbf{h}}_{u,g}[k]. \quad (1)$$

### B. Stage 2: RSMA-based MGM Signal Design

Fig. 1 depicts RSMA-based MGM in operation. Let  $W_1$  and  $W_2$  denote the messages meant for groups 1 and 2, respectively. At the TX, each  $W_g$  ( $g = 1, 2$ ) is split (by the message splitter block) into common and private portions denoted by  $W_{c,g}$  and  $W_{p,g}$ , respectively (i.e.,  $W_g = W_{c,g} \cup W_{p,g}$ ). The two common portions –  $W_{c,1}$  and  $W_{c,2}$  – are then combined (by the message combiner block) into a common message,  $W_c$ . The three message components –  $W_c$ ,  $W_{p,1}$  and  $W_{p,2}$  – are then individually encoded and modulated to form data streams  $s_c[k]$ ,  $s_1[k]$  and  $s_2[k]$ , respectively, over the subcarriers ( $k = 0, \dots, N_c - 1$ ).  $s_c[\cdot]$  is referred to as the *common stream*, whereas  $s_1[\cdot]$  ( $s_2[\cdot]$ ) is referred to as the *private stream* of group 1 (group 2).

The streams are then linearly precoded, giving rise to the transmit signal  $\mathbf{x}[k]$  over the  $k$ -th subcarrier, which can be expressed as follows:

$$\mathbf{x}[k] = \mathbf{p}_c s_c[k] + \mathbf{p}_1 s_1[k] + \mathbf{p}_2 s_2[k]. \quad (2)$$

where  $\mathbf{p}_c$  is referred to as the *common stream precoder* and  $\mathbf{p}_g$  the *private stream precoder* of group  $g$ . Let  $\mathbf{P} := [\mathbf{p}_c, \mathbf{p}_1, \mathbf{p}_2]$  denote the collection of precoders.

**Remark 1.**  $\mathbf{P}$  is designed as a function of the (imperfect) CSIT acquired in Stage 1 [see (8)-(9)]. However, to avoid messy notation, this functional dependence is not shown explicitly.

**Remark 2.** Assuming unit symbol power (i.e.,  $\mathbb{E}[|s_c[k]|^2] = \mathbb{E}[|s_1[k]|^2] = \mathbb{E}[|s_2[k]|^2] = 1$ ),  $\|\mathbf{p}_c\|^2$  and  $\|\mathbf{p}_g\|^2$  represent the power allocated to the common stream and group  $g$ 's private stream, respectively. In (2), the same precoders are applied across all subcarriers, which translates to uniform power allocation over the subcarriers. This suboptimal choice is driven by our use of imperfect CSIT in (1) to design  $\mathbf{P}$ . The optimal power allocation – dictated by waterfilling – requires knowledge of  $\mathbf{h}_{u,g}[k]$  at the TX for all  $k$ .

The received signal at  $(u, g)$ , denoted by  $y_{u,g}[k]$ , is given by:

$$\begin{aligned} y_{u,g}[k] &= \mathbf{h}_{u,g}^H[k] \mathbf{x}[k] + n_{u,g}[k] \\ &= \mathbf{h}_{u,g}^H[k] \mathbf{p}_c s_c[k] + \mathbf{h}_{u,g}^H \mathbf{p}_g s_g[k] + \mathbf{h}_{u,g}^H \mathbf{p}_{g'} s_{g'}[k] \\ &\quad + n_{u,g}[k]. \end{aligned} \quad (3)$$

From the perspective of  $(u, g)$ , the first and second terms in (3) both contain useful information – the former represents the common stream component, a part of which is meant solely for group  $g$  users, while the latter represents the private stream component meant solely for group  $g$  users. In contrast, the third term does not contain useful information, as it captures the private stream component meant for the other group  $g' \neq g$ . Finally,  $n_{u,g}[k] \sim \mathcal{CN}(0, \sigma^2)$  denotes the receiver noise at  $(u, g)$ .

We assume that precoded pilot<sup>3</sup> signals have been interspersed across some subcarriers of  $\mathbf{x}[k]$  to help  $(u, g)$  estimate  $\mathbf{h}_{u,g}^H[k] \mathbf{p}_c$  and  $\mathbf{h}_{u,g}^H[k] \mathbf{p}_g$  upon receiving  $y_{u,g}[k]$ , in order to decode the useful information in the first two terms of (3). Using its estimate of  $\mathbf{h}_{u,g}^H[k] \mathbf{p}_c$ ,  $(u, g)$  first equalizes (3) to decode  $s_c[k]$  and recover  $W_c$ , by treating the second and third (interference) terms in (3) as noise. The decoded estimate of  $W_c$  is simultaneously sent to:

- the message splitter block to extract  $\hat{W}_{c,g}^{(u)}$ , which is the estimate of  $W_{c,g}$  at  $(u, g)$ , and
- the SIC block, which generates an estimate of  $\mathbf{h}_{u,g}^H[k] \mathbf{p}_c s_c[k]$  and subtracts it from  $y_{u,g}[k]$ . Using its estimate of  $\mathbf{h}_{u,g}^H[k] \mathbf{p}_g$ ,  $(u, g)$  then equalizes the resulting residue to decode  $s_g[\cdot]$  and recover  $W_{p,g}$ , while treating the interference from the third term of (3) as noise. Let  $\hat{W}_{p,g}^{(u)}$  denote the decoded estimate of  $W_{p,g}$  at  $u$ . Hence, the estimate of  $W_g$  at  $(u, g)$ , denoted by  $\hat{W}_g^{(u)}$ , is given by  $\hat{W}_g^{(u)} := \hat{W}_{c,g}^{(u)} \cup \hat{W}_{p,g}^{(u)}$ .

Let  $R_{c,g}(\mathbf{P})$  denote the highest (instantaneous) rate (in bits/s/Hz) supporting error-free decoding of  $s_c[\cdot]$  among the users in group  $g$ , under the assumption that  $\hat{\mathbf{h}}_{u,g}$  in (1) constitutes perfect CSIT. It has the following expression:

$$R_{c,g}(\mathbf{P}) := \min_u \log_2 \left( 1 + \frac{|\hat{\mathbf{h}}_{u,g}^H \mathbf{p}_c|^2}{\sigma^2 + \sum_{g=1}^2 |\hat{\mathbf{h}}_{u,g}^H \mathbf{p}_g|^2} \right), \quad (4)$$

where the minimum reflects the fact that every user in group  $g$  must decode  $s_c[\cdot]$ .

**Remark 3** (Achievability). *Strictly speaking,  $R_{c,g}(\mathbf{P})$  is not achievable as it may involve transmitting at a rate that is not supported by the true CSI  $\{\mathbf{h}_{u,g}[k] : \forall k\}$ . The ergodic rate,  $\mathbb{E}_{\mathbf{h}, \hat{\mathbf{h}}}[R_{c,g}(\mathbf{P})]$ , on the other hand is achievable, where the averaging is over the joint distribution of the true CSI and the CSIT [33] (subscripts omitted for simplicity). Since this joint distribution is unknown in practice, the ergodic rate is not a tractable metric for designing  $\mathbf{P}$ . Hence, despite not being technically achievable,  $R_{c,g}(\mathbf{P})$  [and similarly,  $R_{p,g}(\mathbf{P})$  in (6)] is still useful<sup>4</sup> for designing  $\mathbf{P}$  [see  $OP_{\text{mmf}}$  in (8)-(9)]. For such  $\mathbf{P}$ , the empirically achievable rates in our experiments are determined by a suitable choice of modulation and coding scheme (MCS) levels.*

Since  $s_c[\cdot]$  contains useful information for users in *both* groups, it follows that both groups must be able to decode  $s_c[\cdot]$ . Hence, subject to (4), the highest rate supporting error-free decoding of  $s_c[\cdot]$  by both groups – denoted by  $R_c(\mathbf{P})$  and referred to as the *common stream rate* – is given by:

$$R_c(\mathbf{P}) = \min_g R_{c,g}(\mathbf{P}). \quad (5)$$

<sup>3</sup>These pilots play a role similar to the demodulation reference signals (DM-RS) used in LTE and 5G NR.

<sup>4</sup>The ergodic rate,  $\mathbb{E}_{\mathbf{h}, \hat{\mathbf{h}}}[R_{c,g}(\mathbf{P})]$ , can be expressed as  $\mathbb{E}_{\hat{\mathbf{h}}}[\mathbb{E}_{\mathbf{h}}[R_{c,g}(\mathbf{P})]]$ , where the outer expectation is w.r.t the distribution of the CSIT, and the inner expectation is w.r.t the conditional distribution of the true CSI, given the CSIT. As an alternative to the *instantaneous* rate  $R_{c,g}(\mathbf{P})$ , the term  $\mathbb{E}_{\hat{\mathbf{h}}}[R_{c,g}(\mathbf{P})]$  – known as the *average rate* (and in general, not achievable) – can also be used to design  $\mathbf{P}$  as a function of the CSIT [33]. However, like with the ergodic rate, the average rate is also not a tractable metric in practice, since the conditional distribution is unknown and obtaining an empirical estimate at the TX involves considerable overhead.

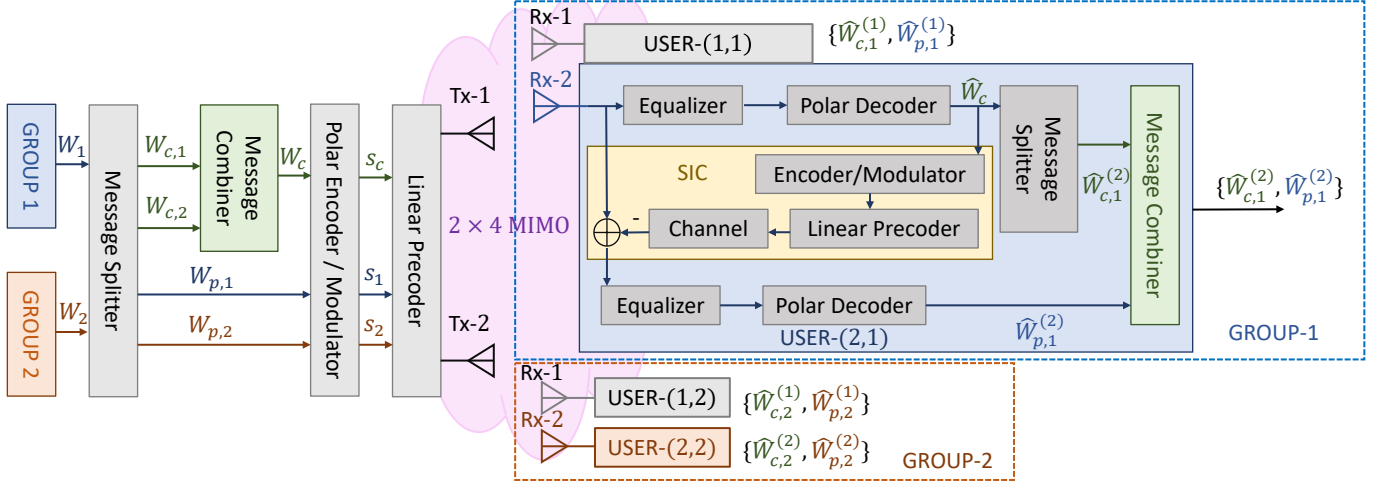


Fig. 1: An illustration of RSMA-based MGM.

After perfect SIC (in other words, assuming  $R_c(\mathbf{P})$  is achievable for all users), let  $R_{p,g}(\mathbf{P})$  denote the highest (instantaneous) rate supporting error-free decoding of  $s_g[\cdot]$  among the users in group  $g$ , again under the assumption that (1) constitutes perfect CSIT. This is referred to as *group  $g$ 's private stream rate* and has an expression similar to (4), given by:

$$R_{p,g}(\mathbf{P}) := \min_u \log_2 \left( 1 + \frac{|\hat{\mathbf{h}}_{u,g}^H \mathbf{P}_g|^2}{\sigma^2 + |\hat{\mathbf{h}}_{u,g}^H \mathbf{p}_{g'}|^2} \right) \quad (g' \neq g). \quad (6)$$

Subject to (5) and (6), the highest rate supporting error-free recovery of  $W_g$  by all users in group  $g$  – denoted by  $R_g(\mathbf{P})$  and referred to as the *net group  $g$  rate* – is given by :

$$R_g(\mathbf{P}) = \frac{|W_{c,g}|}{|W_c|} R_c(\mathbf{P}) + R_{p,g}(\mathbf{P}), \quad (7)$$

where the first term is the fraction of the common message ( $W_c$ ) intended for group  $g$ .

In general, the sizes of  $W_{c,1}$  and  $W_{c,2}$  (in bits) in Fig. 1 need not be equal, which can be used to enable RSMA-based MGM to achieve better fairness. To illustrate this, suppose group 2's private stream rate is smaller than that of group 1 [i.e.,  $R_{p,2}(\mathbf{P}) < R_{p,1}(\mathbf{P})$ ] because group 2 users have weaker channels than group 1 users. In such a scenario, allocating a larger fraction of the common stream to group 2 ( $|W_{c,2}| > |W_{c,1}|$ ) has the effect of driving the net group rates –  $R_1(\mathbf{P})$  and  $R_2(\mathbf{P})$  – towards parity, as captured by the RHS of (7). This motivates the following scheme:

- S1) if  $|R_{p,1}(\mathbf{P}) - R_{p,2}(\mathbf{P})| \leq R_c(\mathbf{P})$ , then the common stream is allocated such that  $R_{p,1}(\mathbf{P}) + (|W_{c,1}|/|W_c|)R_c(\mathbf{P}) = R_{p,2}(\mathbf{P}) + (|W_{c,2}|/|W_c|)R_c(\mathbf{P})$  to ensure that both groups have the same throughput (i.e., achieving max-min fairness);
- S2) otherwise, when  $|R_{p,1}(\mathbf{P}) - R_{p,2}(\mathbf{P})| > R_c(\mathbf{P})$ , the entire common stream is allocated to the group with the smaller private stream rate.

The design of  $\mathbf{P}$  to realize max-min rate fairness across the two groups yields the following optimization problem:

$$OP_{\text{mmf}} : \max_{\mathbf{P}} \min\{R_1(\mathbf{P}), R_2(\mathbf{P})\} \quad (8)$$

$$\text{s.t. } \text{tr}(\mathbf{P}\mathbf{P}^H) \leq P_t, \quad (9)$$

where (9) is the TX power constraint. Due to the non-convexity of  $OP_{\text{mmf}}$ , a tractable algorithm that converges to its global optimal solution does not exist. However, a locally optimal solution that is widely recognized as the gold-standard can be obtained using the *WMMSE method* [24], which takes advantage of the well-known relationship between the achievable rate and the post-equalization symbol mean square error [34]. Let  $\mathbf{P}^{\text{wm}} := [\mathbf{p}_c^{\text{wm}}, \mathbf{p}_1^{\text{wm}}, \mathbf{p}_2^{\text{wm}}]$  denote the solution to  $OP_{\text{mmf}}$  obtained by the WMMSE method. However, the resulting max-min fair rate is difficult to realize in practice because, in addition to Remark 3:

1. Data transmission is typically restricted to a finite collection of MCS levels, which caps the achievable rate/throughput, and
2. Error-free decoding of the streams at any user cannot be guaranteed due to a combination of finite block length effects and CSI estimation errors, which further reduces the measured throughput.

To account for imperfect CSIT, discrete MCS levels and decoding errors, we consider the *MCS-limited* throughput as the metric of interest throughout this paper. An MCS level is defined by a pair  $(m, r)$ , where positive integer  $m$  denotes the bits per constellation symbol (e.g., 2 for QPSK) and  $r \in (0, 1]$  denotes the code rate. Let  $\mathcal{M} := \{(m_c, r_c), (m_1, r_1), (m_2, r_2)\}$  denote the set of MCS levels chosen for  $s_c[\cdot]$ ,  $s_1[\cdot]$  and  $s_2[\cdot]$ , respectively. Then, the corresponding *MCS-limited* throughputs (measured in bits/s) with

WMMSE precoders are given by:

$$T_c^{\text{mcs}}(\mathbf{P}^{\text{wm}}, \mathcal{M}) = Bm_c r_c \times \mathbb{P}(\hat{W}_c = W_c), \quad (10)$$

$$T_{p,1}^{\text{mcs}}(\mathbf{P}^{\text{wm}}, \mathcal{M}) = Bm_1 r_1 \times \mathbb{P}(\hat{W}_{p,1}^{(1)} = \hat{W}_{p,1}^{(2)} = W_{p,1}),$$

$$T_{p,2}^{\text{mcs}}(\mathbf{P}^{\text{wm}}, \mathcal{M}) = Bm_2 r_2 \times \mathbb{P}(\hat{W}_{p,2}^{(1)} = \hat{W}_{p,2}^{(2)} = W_{p,2}).$$

In the above expressions,  $B$  denotes the effective bandwidth<sup>5</sup>, and the probability terms capture the loss in throughput due to decoding errors – specifically, the first expression denotes the probability that  $W_c$  is correctly decoded by all groups, while the second and third expressions denote the probability that  $W_{p,1}$  and  $W_{p,2}$  are correctly decoded by groups 1 and 2, respectively.

**Remark 4.** *The message decoding probabilities in the RHS of (10) are a function of the chosen MCS level, as well as the SINR at each user, which in turn, depends on  $\mathbf{P}^{\text{wm}}$ . This functional dependence is not shown explicitly to avoid messy notation.*

Similar to (7), the MCS-limited throughput for group  $g$  with WMMSE precoders is given by :

$$T_g^{\text{mcs}}(\mathbf{P}^{\text{wm}}, \mathcal{M}) = \frac{|W_{c,g}|}{|W_c|} T_c^{\text{mcs}}(\mathbf{P}^{\text{wm}}, \mathcal{M}) + T_{p,g}^{\text{mcs}}(\mathbf{P}^{\text{wm}}, \mathcal{M}) \quad (11)$$

Thus, similar to  $OP_{\text{mmf}}$  in (8)-(9), the MCS-limited max-throughput fairness problem for RSMA-based MGM, which is of considerable practical relevance, can be defined as follows:

$$OP_{\text{mmf}}^{\text{mcs}} : \max_{\mathcal{M}} \min\{T_1^{\text{mcs}}(\mathbf{P}^{\text{wm}}, \mathcal{M}), T_2^{\text{mcs}}(\mathbf{P}^{\text{wm}}, \mathcal{M})\} \quad (12)$$

$$\text{s.t. } \mathcal{M} \in \mathbb{M}, \quad (13)$$

where  $\mathbb{M}$  denotes the collection of permissible MCS levels for the three streams, which is typically pre-determined through standards (see Table II for the  $\mathbb{M}$  used in our measurements). The optimal  $\mathcal{M}$  for  $OP_{\text{mmf}}^{\text{mcs}}$  is a function of  $\mathbf{P}^{\text{wm}}$  that is difficult to characterize because the message decoding probabilities in (10) do not have closed-form expressions in terms of  $\mathbf{P}^{\text{wm}}$  and  $\mathcal{M}$ . However, these probabilities can be empirically evaluated through measurements. This motivates us to *empirically solve*  $OP_{\text{mmf}}^{\text{mcs}}$  through a brute force search<sup>6</sup> over  $\mathbb{M}$ , which is the focus of our measurements in Section IV.

We conclude this subsection by noting SDMA- and NOMA-based MGMs are special cases of RSMA-based MGM, corresponding to specific choices of message splitting, as explained in the following remarks.

**Remark 5.** *SDMA-based MGM is a special case of RSMA-based MGM, where the common stream is turned off – i.e.,  $W_g = W_{p,g}$ , ( $g = 1, 2$ ) in Fig. 1. The corresponding expressions in (2)-(13) for SDMA-based MGM can be obtained by setting  $\mathbf{p}_c = \mathbf{0}$ . Essentially, without a common stream,*

<sup>5</sup>The effective bandwidth is the portion of the total bandwidth available for data transferring, after accounting for signalling overhead (e.g., the cyclic prefix in OFDM, pilot subcarriers and guard band in IEEE 802.11 standard)

<sup>6</sup>A more sophisticated empirical approach involves link adaptation, where the most suitable MCS level is determined by an ARQ-based mechanism [35]. This is left for future work.

	Name	Description
1.	Workstation	Running LabVIEW NXG
2.	NI USRP-2942 (3 units)	SDRs used to realize TX and users
3.	NI CPS-8910	Provides additional PCIe ports
4.	NI CDA-2990	8 Channel, 10 MHz clock distribution device
5.	8dBi RP-SMA Male Wifi Antenna	TX antennas
6.	RP-SMA Male Wifi Antenna	Group 1 users' antennas
7.	Mini-Circuits ZAPD-272-S+	Power splitter
8.	TP-Link TL-ANT2405C	Group 2 users' antennas

TABLE I: List of hardware components.

group  $g$  users treat the interference from  $W_{g'}$  ( $g' \neq g$ ) as noise.

**Remark 6.** *NOMA-based MGM is a special case of RSMA-based MGM, where the private stream message of one group (group 2, say) is turned off (i.e.,  $W_{p,2} = \emptyset$ ), and no portion of the other message is allocated to the common stream (i.e.,  $W_1 = W_{p,1}$ ,  $W_2 = W_{c,2} = W_c$  in Fig. 1). The corresponding expressions in (2)-(13) can be obtained by setting  $\mathbf{p}_2 = \mathbf{0}$ . For this example, group 1 users fully decode and subtract the interference from  $W_2$ , whereas group 2 users treat the interference from  $W_1$  as noise. In contrast, for RSMA-based MGM, group  $g$  users partially decode the interference from  $W_{g' \neq g}$  ( $W_{c,g'}$ ) and partially treat it as noise ( $W_{p,g'}$ ).*

**Remark 7.** *The common stream allocation, as per condition S2 on page 4, is similar to NOMA-based MGM, albeit the weaker group also has a private stream.*

### III. RSMA PROTOTYPE

#### A. Hardware setup

We implement RSMA-based MGM by using our Software Defined Radio (SDR) based RSMA prototype [26]. The TX and RXs are realized using National Instruments' (NI) USRP 2942 SDR units, which have two antennas/RF chains. Hence, we use three USRP 2942 units, one to realize a two-antenna TX ( $N_t = 2$ ), and the other two to realize four single-antenna users that are assigned to two groups of two users each in our measurements in Section IV. In particular, the antennas of group 2 users are connected to their USRP through coaxial cables, which allow them to be moved around to realize different channel environments, as described in Section IV-A. The USRPs share a common timing source (CDA-2990), and are controlled by a workstation running LabVIEW NXG, through which the various blocks in Fig. 1 are realized. All connections (SDRs to workstation, SDRs to timing sources) are through PCIe cables, facilitated by a PCIe bus (CPS-8910). A list of hardware components is provided in Table I.

#### B. RSMA-based MGM Implementation

We adopt several features of the IEEE 802.11g physical layer frames to implement the system model described in Section II.

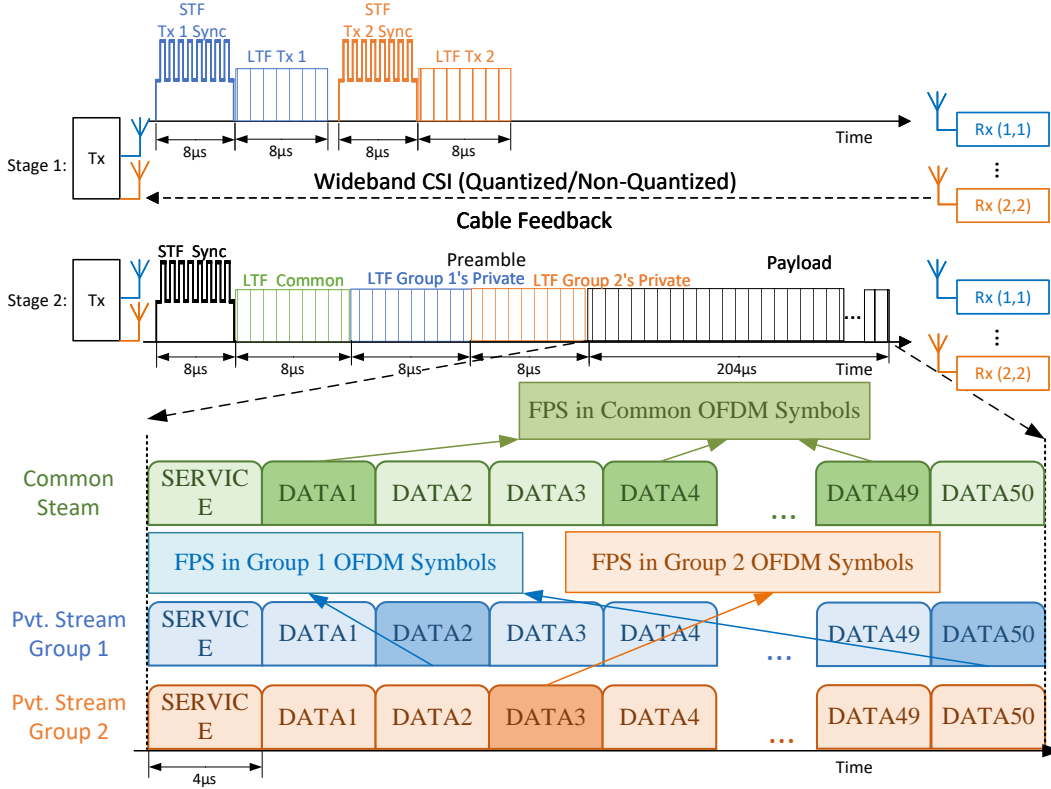


Fig. 2: Signal structure within the two-stage transmission protocol used to implement RSMA-based MGM. In conventional 802.11g, every DATA (OFDM) symbol for a user contains four pilot subcarriers for FPS. However, for RSMA-based MGM, this approach would cause the pilot subcarriers in the common and private streams to interfere with each other. To avoid this, the three streams carry non-zero pilots orthogonally once every three OFDM symbols, as shown above.

*a) Stage 1:* Each TX antenna transmits a pilot signal orthogonally in time comprising a Short Training Field (STF,  $8\mu\text{s}$  in duration) and a Long Training Field (LTF,  $8\mu\text{s}$  in duration), as shown in the top portion of Fig. 2. The STF is used for synchronization and coarse frequency offset estimation, while the LTF is used for CSI estimation at each user (i.e.,  $\hat{\mathbf{h}}_{u,g}[k]$  in Section II-A).

*b) Stage 2:* The transmitted signal consists of a preamble followed by the data payload, as shown in the bottom portion of Fig. 2.

- **Preamble:** The preamble consists of one STF and three LTFs. The function of the STF is the same as in Stage 1, while the LTFs are precoded in order to estimate the *precoded CSI* for equalization at the users. The first LTF is used by each  $(u, g)$  to estimate  $\mathbf{h}_{u,g}^H \mathbf{p}_c$  for decoding the common stream. The second LTF is used by each user  $u$  in group 1 to estimate  $\mathbf{h}_{u,1}^H \mathbf{p}_1$  to decode its private stream. Similarly, the third LTF is used by each user  $u'$  in group 2 to estimate  $\mathbf{h}_{u',2}^H \mathbf{p}_2$  to decode its private stream.
- **Data Payload:** For the payload, we consider a total bandwidth of 20MHz with  $N_c = 64$  subcarriers and a cyclic prefix (CP) of 16 samples per OFDM symbol. Aligned with IEEE 802.11 frames, 52 subcarriers are used for communications while the rest serve as guard bands. Among these 52 subcarriers, 48 are used to carry data symbols, with the remaining used to correct the common

phase error across all subcarriers in one OFDM symbol [36]. This yields an effective bandwidth of:

$$B = 20\text{MHz} \times \underbrace{\left(\frac{64}{80}\right)}_{\text{CP overhead}} \times \underbrace{\left(\frac{48}{64}\right)}_{\text{Guard band overhead}} = 12\text{MHz} \quad (14)$$

The payload consists of three superposed streams (one common, two private), each comprising 50 OFDM symbols.

- **MCS Implementation:** Table II lists the MCS levels,  $\mathbb{M}$ , implemented in our prototype. For channel coding, we implement Polar codes augmented with an 8-bit cyclic redundancy check [37], [38], along with successive cancellation list decoding [39], with a list depth of 2. After the preamble, the first OFDM symbol (labelled SERVICE in the bottom portion of Fig. 2) contains the MCS information of each stream.

An instance of Stage 1 and Stage 2, as described above and illustrated in Fig. 2, constitutes a single measurement run. To empirically solve  $OP_{\text{mmf}}^{\text{mcs}}$ , we conduct 100 measurement runs. Let  $D_c$  denote the number of runs in which the common stream is successfully decoded by all users. Similarly, let  $D_g$  ( $g \in \{1, 2\}$ ) denote the number of runs in which both users in group  $g$  successfully decode their private stream. Replacing the message decoding probabilities in (10) with

MCS Index	Modulation ( $m$ )	Code Rate $r$	Data Rate $Bmr$ (Mbps)
0	BPSK (1)	1/2	6
1	BPSK (1)	3/4	9
2	QPSK (2)	1/2	12
3	QPSK (2)	3/4	18
4	16QAM (4)	1/2	24
5	16QAM (4)	3/4	36
6	64QAM (6)	2/3	48
7	64QAM (6)	3/4	54
8	256QAM (8)	3/4	72
9	256QAM (8)	5/6	80

TABLE II: MCS levels (largely based on IEEE 802.11g) implemented in our prototype. The data rate in the last column is equal to  $Bmr$ , where  $B$  is the effective bandwidth given by (14).

their empirical estimates, the *measured* common and private stream throughputs for RSMA-based MGM is given by:

$$\begin{aligned}
T_c^{\text{mcs}}(\mathbf{P}^{\text{wm}}, \mathcal{M}) &= \frac{D_c}{100} Bm_c r_c, \\
T_{p,1}^{\text{mcs}}(\mathbf{P}^{\text{wm}}, \mathcal{M}) &= \frac{D_1}{100} Bm_1 r_1, \\
T_{p,2}^{\text{mcs}}(\mathbf{P}^{\text{wm}}, \mathcal{M}) &= \frac{D_2}{100} Bm_2 r_2,
\end{aligned} \quad (15)$$

where  $B$  is given by (14) and the MCS levels are chosen from Table II.

Parameter	Notation	Value
Center frequency	$f_c$	2.484GHz <sup>7</sup>
Transmit power	$P_t$	23dBm
No. of groups		2
No. of users per group		2
Total bandwidth		20MHz
Subcarriers	Total ( $N_c$ )	64
	Data	48
	Pilot (FPS)	4
	Guard band	12
CP length		16
Effective bandwidth	$B$	12MHz
OFDM symbols in payload		50
Experiment runs (per case)		100
TX antenna spacing		0.13m
Fraunhofer distance		0.28m
Distance between Group-1 RXs and TX		1.00m
Distance between Group-2 RXs and TX	Case 1-3	1.00-1.50m
	Case 4-6	2.00-2.30m
	Case 7-9	3.20-3.50m

TABLE III: List of parameters used in our experiments.

## IV. RESULTS

### A. Measurement setup

In MGM, it is well known that a group's throughput is limited by its *weakest* user. Hence, in the existing literature, there is an assumption of admission control during the formation of the groups, so that users within a group have similar channel strength/link SNR. This motivates us to focus on the scenario where users within a group are closely situated, which could occur in applications like gaming, video

<sup>7</sup>This value corresponds to channel no. 14 in the IEEE 802.11 family of standards for the 2.4GHz band. We use this channel to avoid ambient WiFi interference, as it is not commercially used in the UK.

conferencing, etc. In such cases, users within a group are likely to experience similar pathloss, whereas there could be considerable pathloss differences across groups. Furthermore, as the relative performance of SDMA-, NOMA- and RSMA-based MGM is a function of the inter-group interference, it is important to realize a range of environments with varying levels of inter-group interference for a meaningful three-way comparison. This is intrinsically challenging for MGM, as notions of *weak/medium/strong* interference need to be defined over four pairs of links across the two groups instead of a single pair of links for two-user unicast. Motivated by our unicast measurements [26, Section IV], we rely on geometric notions of channel spatial correlation in line-of-sight environments as a predictor of inter-group interference levels. Thus, similar to [26], we consider nine measurement cases, as illustrated in Fig. 3a, where moving in the horizontal direction *should* increase the inter-group pathloss difference, while moving in the vertical direction is *should* decrease the spatial correlation (and in turn, the interference levels) between the groups.

To quantify the inter-group pathloss difference between user  $u$  in group 1 and user  $u'$  in group 2, we define a parameter,  $\alpha_{u,u'}$  (in dB scale) as follows:

$$\alpha_{u,u'} \text{ [dB]} = 10 \log_{10} \frac{\|\hat{\mathbf{h}}_{u',2}\|}{\|\hat{\mathbf{h}}_{u,1}\|}, \quad (16)$$

where  $\hat{\mathbf{h}}_{u,g}$  is given by (1). Since group 2 is farther from the TX than group 1, a large negative value signifies greater pathloss difference among the two groups. Likewise, let  $\rho_{u,u'}$  denote the spatial correlation between users  $u$  in group 1 and  $u'$  in group 2, which is defined as follows:

$$\rho_{u,u'} = \frac{|\hat{\mathbf{h}}_{u,1}^H \hat{\mathbf{h}}_{u',2}|}{\|\hat{\mathbf{h}}_{u,1}\| \cdot \|\hat{\mathbf{h}}_{u',2}\|}. \quad (17)$$

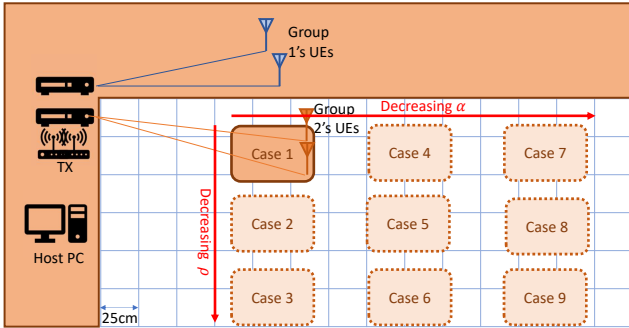
Thus,  $\rho_{u,u'} = 1$  signifies fully correlated (i.e., highly interfering) channels, while  $\rho_{u,u'} = 0$  signifies orthogonal (i.e., zero interference) channels. The intuitive directions of decreasing  $\alpha$  and  $\rho$  are marked in Fig. 3a.

To realize Fig. 3a, group 1 users are fixed on a workbench 1m from the TX, while group 2 users are placed on a trolley (Fig. 3b) and moved around to realize the nine cases. The distance between the TX and group 2 is provided in Table III. All users are in the far field. Table IV captures the spread of the four  $\alpha$  and  $\rho$  values for the nine cases. While the  $\alpha$  spread is fairly narrow and follows the expected trend shown in Fig. 3a, the  $\rho$  spread is much larger for several cases because the intuition behind strong/medium/high levels of inter-group spatial correlation in Fig. 3a was based on only the (dominant) line-of-sight component, whereas the measured  $\rho$  is also sensitive to multipath, which is uncorrelated for each user. This highlights the difficulty of precisely controlling the extent of inter-group interference. Nevertheless, a shift towards 1 in the  $\rho$  spread consistent with increasing spatial correlation can be discerned when looking at the low and medium category of cases. No such insight can be drawn from the medium and high categories.

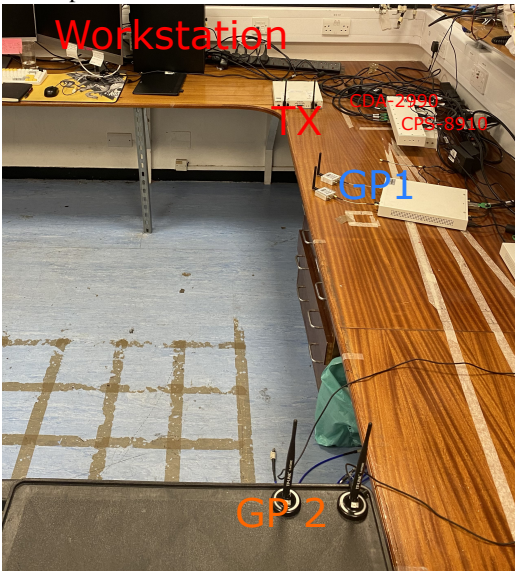
A full list of parameters used in our experiments is provided in Table III.

	Inter-group Pathloss Difference		Inter-group Spatial Correlation	
	Case	$\alpha$ spread [-20,0]	Case	$\rho$ spread [0,1]
Low	1		3	
	2		6	
	3		9	
Medium	4		2	
	5		5	
	6		8	
High	7		1	
	8		4	
	9		7	

TABLE IV: The rectangles in the third and last columns capture the spread of the measured inter-group pathloss difference ( $\alpha_{u,u'}$ ) and inter-group spatial correlation ( $\rho_{u,u'}$ ). The left (right) end of each rectangle corresponds to the smallest (largest) value for each case. As expected, the  $\alpha$  spread becomes more negative as the pathloss difference between the groups increases. But, the  $\rho$  spread is large for several cases due to sensitivity to multipath. Despite this, a shift towards 1 consistent with increasing spatial correlation can be discerned when looking at the low and medium categories of cases.



(a) The layout of the measurement environment, along with the TX and user positions for the nine cases.



(b) The measurement environment (Case 4 is shown here).

Fig. 3: Measurement setup

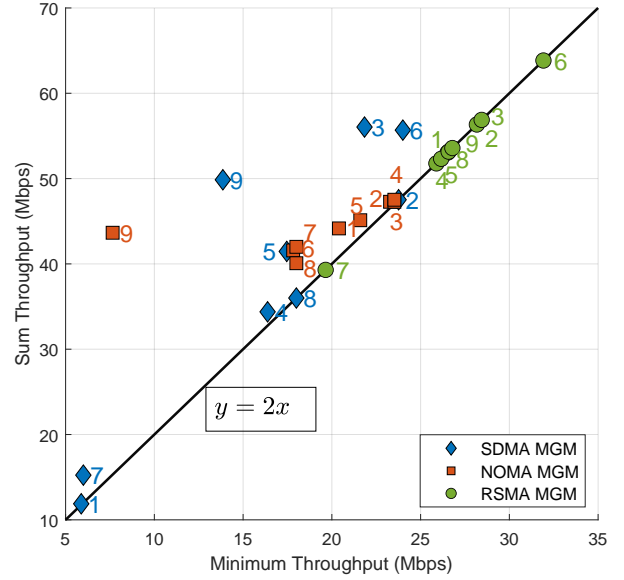


Fig. 4: Fairness comparison between SDMA-based, NOMA-based and RSMA-based MGM. The number beside each data point indicates the measurement case. The black line ( $y = 2x$ ) corresponds to max-min fairness, and points that are closer (in terms of Euclidean distance) to this line represent fairer outcomes.

### B. Fairness Comparison

To compare the fairness performance of RSMA-, NOMA- and SDMA-based MGM, Fig. 4 plots the sum throughput versus the minimum throughput for each case. The case number is indicated beside each data point. The black  $y = 2x$  line represents max-min fairness, and the region above is feasible for all three multiple access schemes. Thus, points that are closer (in terms of Euclidean distance) to the black line represent *fairer* outcomes. Furthermore, a point that is either to the north, northeast or east of another point represents a *better* outcome. Based on these insights, we make the following observations:

- SDMA: From the spatial geometry of the user locations, cases 1, 4 and 7 have the highest amount of inter-group interference. For these cases, SDMA-based MGM achieves significantly lower minimum and sum throughput than NOMA- and RSMA-based MGM despite achieving near fairness. This is borne by the fact that the SDMA points for these cases lie to the southwest of the corresponding NOMA/RSMA points roughly along the  $y = 2x$  line. This validates the well-known limitation of treating interference as noise in the high interference regime.
- NOMA: With the exception of Case 9, NOMA-based MGM either achieves or comes close to achieving fairness for the other cases. It also achieves better outcomes than SDMA for cases 1, 4, 5, 7 and 8. Interestingly, it achieves strictly *worse* outcomes than SDMA for cases 3, 6, and 9, despite SDMA's limitations on interference suppression in an overloaded scenario. It's worth noting that these cases are associated with the lowest inter-group



interference (due to the relatively lower inter-group spatial correlation). This suggests that even for overloaded scenarios where interference cannot be fully suppressed to noise levels, a flexible mix of (partially) decoding the interference and (partially) treating it as noise, in response to the channel conditions is the ideal interference strategy, something RSMA achieves by design.

- RSMA: In Section II, when condition S1 (see page 4) is true, the corresponding RSMA-based MGM point lies on the  $y = 2x$  (i.e., achieves max-min fairness). Otherwise, for condition S2, the RSMA point lies *as close as possible* above the black line. For all cases, RSMA achieves max-min fairness, thereby implying that S1 is satisfied for each case (more on this while discussing Fig. 5). Furthermore, compared to SDMA, RSMA achieves strictly better performance for all cases. Likewise, when compared to NOMA, RSMA achieves strictly better performance for all cases bar one – the exception being case 7, where NOMA achieves a higher sum throughput than RSMA but not fairness (see Section IV-C-c for an explanation). To explain RSMA’s superior performance w.r.t SDMA and NOMA, it’s important to gain some insight into the relative contributions of the common and private streams to each group’s net throughput for each case. We will elaborate on this next.

Complementing Fig. 4, Fig. 5 plots the throughput of each group. For RSMA-based MGM, a group’s throughput is broken down into common and private stream contributions. The arrows indicate the gain in the minimum throughput due to RSMA-based MGM. We make the following observations:

- In each subfigure, the contribution of the common stream to each group’s throughput decreases from left to right across the three cases. This pattern was observed for unicast communications, as well [26]. Essentially, when the inter-group interference is high (as in cases 1, 4 and 7), most of the power is allocated to the common stream, which, in turn, contributes substantially to the net throughput. In other words, decoding most of the interference is favoured over suppressing it to noise levels. On the other hand, when the inter-group interference is lower (as in cases 3, 6 and 9), suppressing most of the interference to noise levels is preferred and hence, the power allocation to the private streams increases. As a result, the private streams contribute more to the net throughput.
- For RSMA-based MGM, there is a non-zero common stream contribution to each group’s throughput in every case. Thus, S1 (see page 4) is satisfied for each case, and the allocation of the common stream to each group is done to ensure that both groups have the same net throughput. In other words, throughput contributions from both the common and the private streams for each group provides the required flexibility in terms of resource allocation to ensure that fairness is realized for each case.
- To further highlight the benefits of throughput contributions from both the common and the private streams for each group, consider cases 1 and 7 for RSMA-

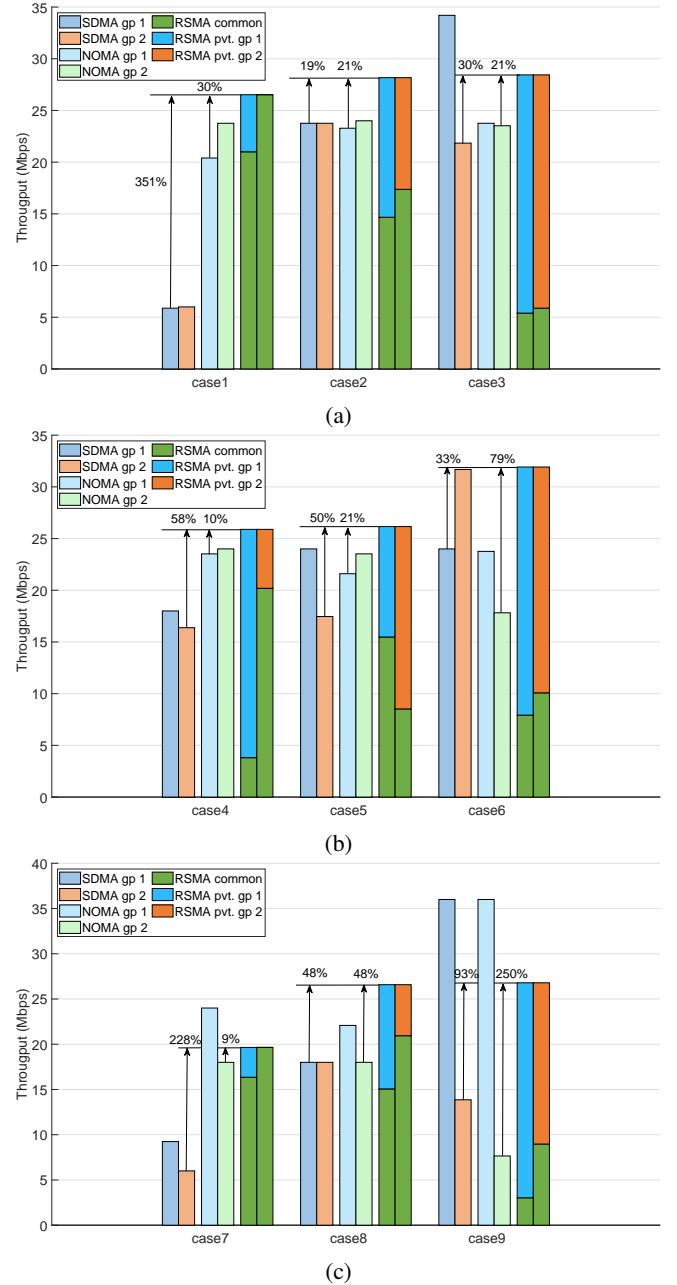


Fig. 5: The throughput performance for both multicast groups of SDMA-, NOMA- and RSMA-based MGM.

based MGM. Since the private stream contribution to (the weaker) group 2’s throughput is zero, it appears at first glance as though RSMA-based MGM reduces to NOMA-based MGM. But there is a key difference. Unlike NOMA, the common stream can contribute to (the stronger) group 1’s throughput as well, to the extent that most of group 1’s throughput is due to the common stream. This is intuitive, since under high inter-group interference, most of the power is allocated to the common stream. In contrast, for NOMA-based MGM, group 1 needs to rely entirely on its private stream for its throughput. This forces a suboptimal resource allocation, where power has to be diverted from the common stream

to group 1's private stream to achieve fairness. As a result, NOMA-based MGM achieves a lower minimum throughput than RSMA-based MGM for these cases. The flexibility offered by throughput contributions from both the common and the private streams for each group is also why RSMA-based MGM achieves better outcomes than both SDMA- and NOMA-based MGM.

In summary, RSMA-based MGM adapts well to variations in pathloss difference and interference between the groups and achieves superior fairness performance (i.e., fairness at a higher minimum throughput) when compared to SDMA- and NOMA-based MGM. We conclude this section by remarking on some seemingly counter-intuitive results in Fig. 5.

### C. Counter-intuitive Results

a) *SDMA, Case 6:* Perhaps the most counter-intuitive observation in Fig. 5 is the supposedly weaker group 2 having a higher throughput (31.68Mbps) than the stronger group 1 (24Mbps) for SDMA-based MGM in Case 6. Table V lists the MCS levels and the block error rate (BLER) associated with each bar in Fig. 5, and the values corresponding to this particular case are:

- Group 1: 16QAM, rate 1/2 (level 4 in Table II) with 0 BLER
- Group 2: 16QAM, rate 3/4 (level 5 in Table II) with 0.12 BLER

It is clear from above that group 2's higher throughput stems from its ability to support a higher MCS level than group 1, albeit it is only one level higher and not error-free. The higher MCS level is due to the fact that more power is allocated to the group 2 precoder to achieve fairness. Ideally, under perfect CSIT, one would expect more power to be allocated to the group 2 precoder in such a way that both groups support the *same* MCS level, thereby achieving the same throughput. However, with imperfect CSIT, which is inherent in our experiments due to the use of wideband CSI in (1), we reckon it is not unusual for group 2 to support an MCS level one higher than group 1. Moreover, if we had imposed strict reliability requirements (i.e., zero BLER in our measurements), then both groups would have supported the same MCS level (16QAM, rate 1/2) and achieved the same throughput.

b) *NOMA, Cases 1, 2, 4 and 5:* Again, group 2 has a higher throughput than group 1 for these cases, although the difference is not as stark as above. This is because both groups support the same MCS level (see Table V) which is expected, but the throughput variations are due to block errors that are difficult to control.

c) *NOMA v/s RSMA, Case 7:* For NOMA-based MGM, groups 1 and 2 supports MCS levels 4 and 3, respectively (both with zero BLER, see Table V), and the resulting sum throughput is 42Mbps. Due to the high pathloss difference and the high inter-group interference associated with this case, RSMA-based MGM reduces to NOMA-based MGM, as evidenced by the lack of a private stream for group 2 (see Remark 6). But, unlike NOMA, the RSMA common stream can contribute to the throughput of *both* groups. Hence, nearly

all of the transmit power is allocated to the common stream precoder. Consequently, the common stream alone should be able to support an MCS level whose throughput is at least 42Mbps (i.e., the NOMA sum throughput), which would then be equally split between the two groups to achieve fairness. However, from Table II, we see that there is no MCS level close to 42Mbps. Hence, in Table V, we see that the common stream supports MCS level 5 (36Mbps) which is the nearest level lower than 42Mbps, but not MCS level 6 (48Mbps) which is the nearest level above 42Mbps. This is the reason why the NOMA sum throughput exceeds the RSMA sum throughput. However, even with conservative MCS level 5 for the common stream, RSMA-based MGM achieves a higher minimum throughput than NOMA-based MGM, which is the desired objective.

## V. CONCLUSION

In this paper, we presented the first-ever experimental evaluation of the fairness performance of RSMA-, SDMA- and NOMA-based MGM. We focused our attention on the overloaded scenario with closely located group members, which is relevant for many applications. For two groups with two users per group, we realized nine cases that captured varying levels of interference and pathloss difference between the two groups. Over these nine cases, we observed that RSMA-based MGM achieved superior fairness performance (i.e., fairness at a higher minimum throughput) than SDMA- and NOMA-based MGM. This is consistent with theoretical predictions. The secret behind these gains stems from the fact that each group's throughput could, in general, have contributions from *both* the common and the private streams with the exact amounts of each dictated by the channel conditions.

## REFERENCES

- [1] B. Elmali, D. M. Soleymani, and S. A. Ashraf, "Empowering public safety services using multicast in 5G-Advanced," *Nokia Blog*, Jan. 2024. [Online]. Available: <https://www.nokia.com/blog/empowering-public-safety-services-using-multicast-in-5g-advanced/>
- [2] 3GPP TS 26.517, "5G Multicast-Broadcast User Services; Protocols and Formats (rel. 17)," Sep. 2023.
- [3] M. Á. Vázquez, A. Pérez-Neira, D. Christopoulos, S. Chatzinotas, B. Ottersten, P.-D. Arapoglou, A. Ginesi, and G. Taricco, "Precoding in Multibeam Satellite Communications: Present and Future Challenges," *IEEE Trans. Wireless Commun.*, vol. 23, no. 6, pp. 88–95, 2016.
- [4] G. Araniti, M. Condoluci, P. Scopelliti, A. Molinaro, and A. Iera, "Multicasting over Emerging 5G Networks: Challenges and Perspectives," *IEEE Network*, vol. 31, no. 2, pp. 80–89, 2017.
- [5] E. Karipidis, N. D. Sidiropoulos, and Z.-Q. Luo, "Quality of service and max-min fair transmit beamforming to multiple cochannel multicast groups," *IEEE Trans. Signal Process.*, vol. 56, no. 3, pp. 1268–1279, 2008.
- [6] T.-H. Chang, Z.-Q. Luo, and C.-Y. Chi, "Approximation bounds for semidefinite relaxation of Max-Min-Fair multicast transmit beamforming problem," *IEEE Trans. Signal Process.*, vol. 56, no. 8, pp. 3932–3943, 2008.
- [7] D. Christopoulos, S. Chatzinotas, and B. Ottersten, "Weighted fair multicast multigroup beamforming under per-antenna power constraints," *IEEE Trans. Signal Process.*, vol. 62, no. 19, pp. 5132–5142, 2014.
- [8] M. Dong and Q. Wang, "Multi-group multicast beamforming: Optimal structure and efficient algorithms," *IEEE Trans. Signal Process.*, vol. 68, pp. 3738–3753, 2020.
- [9] E. Karipidis, N. D. Sidiropoulos, and Z.-Q. Luo, "Far-field multicast beamforming for uniform linear antenna arrays," *IEEE Trans. Signal Process.*, vol. 55, no. 10, pp. 4916–4927, 2007.

Case	BLER (MCS index from Table II)													
	SDMA				NOMA				RSMA					
	Group 1		Group 2		Group 1		Group 2		Common	Group 1 pvt.	Group 2 pvt.			
1	0.02	(0)	0	(0)	0.15	(4)	0.01	(4)	0.01	(6)	0.08	(0)	–	–
2	0.01	(4)	0.01	(4)	0.03	(4)	0	(4)	0.10	(5)	0.25	(3)	0.10	(2)
3	0.05	(5)	0.09	(4)	0.01	(4)	0.02	(4)	0.06	(2)	0.04	(4)	0.06	(4)
4	0	(3)	0.09	(3)	0.02	(4)	0	(4)	0	(4)	0.08	(4)	0.05	(0)
5	0	(4)	0.03	(3)	0.11	(4)	0.02	(4)	0	(4)	0.11	(2)	0.02	(3)
6	0	(4)	0.12	(5)	0.01	(4)	0.01	(3)	0	(3)	0	(4)	0.09	(4)
7	0.23	(2)	0	(0)	0	(4)	0	(3)	0	(5)	0.45	(0)	–	–
8	0	(3)	0	(3)	0.08	(4)	0	(3)	0	(5)	0.04	(2)	0.06	(0)
9	0	(5)	0.23	(3)	0	(5)	0.15	(1)	0	(2)	0.01	(4)	0.01	(3)

TABLE V: The MCS Index and the BLER corresponding to each throughput bar in Fig. 5.

- [10] W. Wang, A. Liu, Q. Zhang, L. You, X. Gao, and G. Zheng, "Robust multigroup multicast transmission for frame-based multi-beam satellite systems," *IEEE Access*, vol. 6, pp. 46 074–46 083, 2018.
- [11] N. Bornhorst, M. Pesavento, and A. B. Gershman, "Distributed beamforming for multi-group multicasting relay networks," *IEEE Transactions on Signal Processing*, vol. 60, no. 1, pp. 221–232, 2012.
- [12] D. Christopoulos, S. Chatzinotas, and B. Ottersten, "Multicast multigroup precoding and user scheduling for frame-based satellite communications," *IEEE Trans. Wireless Commun.*, vol. 14, no. 9, pp. 4695–4707, Sep. 2015.
- [13] X. Zhu, C. Jiang, L. Yin, L. Kuang, N. Ge, and J. Lu, "Cooperative multigroup multicast transmission in integrated terrestrial-satellite networks," *IEEE J. Sel. Areas Commun.*, vol. 36, no. 5, pp. 981–992, 2018.
- [14] Y. C. B. Silva and A. Klein, "Linear transmit beamforming techniques for the multigroup multicast scenario," *IEEE Trans. Veh. Technol.*, vol. 58, no. 8, pp. 4353–4367, Oct 2009.
- [15] N.-D. Nguyen, R. Knopp, N. Nikaein, and C. Bonnet, "Implementation and validation of multimedia broadcast multicast service for LTE/LTE-advanced in OpenAirInterface platform," in *Proc. of the 38th Annual IEEE Conf. on Local Computer Networks (Workshops)*, Oct. 2013, pp. 70–76.
- [16] D. Dujovne and T. Turtletti, "Multicast in 802.11 WLANs: an experimental study," in *Proc. of the 9th ACM Intl. Symp. on Modeling, Analysis and Simulation of Wireless and Mobile Systems*, 2006, p. 130–138.
- [17] M. F. Hanif, Z. Ding, T. Ratnarajah, and G. K. Karagiannidis, "A Minorization-Maximization method for optimizing sum rate in the downlink of non-orthogonal multiple access systems," *IEEE Trans. Signal Process.*, vol. 64, no. 1, pp. 76–88, 2016.
- [18] Z. Wang, J. Hu, G. Liu, and Z. Ma, "Optimal power allocations for relay-assisted NOMA-based 5G V2X broadcast/multicast communications," in *Proc. of the IEEE/CIC Intl. Conf. on Commun. in China (ICCC)*, 2018, pp. 688–693.
- [19] S. M. Iviri, M. Caus, M. A. Vazquez, M. R. Soleymani, Y. R. Shayan, and A. I. Perez-Neira, "Power allocation and user clustering in Multicast NOMA based satellite communication systems," in *Proc. of the IEEE Intl. Conf. on Commun. (ICC)*, 2020, pp. 1–6.
- [20] A. Ihsan, W. Chen, S. Zhang, and S. Xu, "Energy-efficient NOMA multicasting system for beyond 5G cellular V2X communications with imperfect CSI," *IEEE Trans. Intell. Transp. Syst.*, vol. 23, no. 8, pp. 10 721–10 735, 2022.
- [21] J. Choi, "Minimum power multicast beamforming with superposition coding for multiresolution broadcast and application to NOMA systems," *IEEE Trans. Commun.*, vol. 63, no. 3, pp. 791–800, 2015.
- [22] Y. Zhang, T.-X. Zheng, Q. Yang, H.-M. Wang, B. Wang, and Z. Li, "The application of Non-Orthogonal Multiple Access in 5G Physical-Layer Multi-Region geocast," in *2017 IEEE Wireless Communications and Networking Conference (WCNC)*, 2017, pp. 1–6.
- [23] B. Clerckx, Y. Mao, R. Schober, E. A. Jorswieck, D. J. Love, J. Yuan, L. Hanzo, G. Y. Li, E. G. Larsson, and G. Caire, "Is NOMA efficient in multi-antenna networks? A critical look at next generation multiple access techniques," *IEEE Open Journal of the Communications Society*, vol. 2, pp. 1310–1343, 2021.
- [24] H. Joudeh and B. Clerckx, "Rate-Splitting for Max-Min fair multigroup multicast beamforming in overloaded systems," *IEEE Trans. Wireless Commun.*, vol. 16, no. 11, pp. 7276–7289, 2017.
- [25] Y. Mao, O. Dizdar, B. Clerckx, R. Schober, P. Popovski, and H. V. Poor, "Rate-Splitting Multiple Access: Fundamentals, Survey, and Future Research Trends," *IEEE Commun. Surveys Tuts.*, 2022.
- [26] X. Lyu, S. Aditya, J. Kim, and B. Clerckx, "Rate-Splitting Multiple Access: The First Prototype and Experimental Validation of its Superiority over SDMA and NOMA," *IEEE Trans. Wireless Commun.*, pp. 1–1, 2024.
- [27] B. Clerckx, Y. Mao, E. A. Jorswieck, J. Yuan, D. J. Love, E. Erkip, and D. Niyato, "A Primer on Rate-Splitting Multiple Access: Tutorial, Myths, and Frequently Asked Questions," *IEEE J. Sel. Areas Commun.*, vol. 41, no. 5, pp. 1265–1308, May 2023.
- [28] A. Z. Yalcin, M. Yuksel, and B. Clerckx, "Rate splitting for multigroup multicasting with a common message," *IEEE Trans. Veh. Technol.*, vol. 69, no. 10, pp. 12 281–12 285, Oct 2020.
- [29] L. Yin and B. Clerckx, "Rate-splitting multiple access for multigroup multicast and multibeam satellite systems," *IEEE Trans. Commun.*, vol. 69, no. 2, pp. 976–990, Feb 2021.
- [30] H. Chen, D. Mi, T. Wang, Z. Chu, Y. Xu, D. He, and P. Xiao, "Rate-splitting for multicarrier multigroup multicast: Precoder design and error performance," *IEEE Trans. Broadcast.*, vol. 67, no. 3, pp. 619–630, 2021.
- [31] L. Yin, O. Dizdar, and B. Clerckx, "Rate-splitting multiple access for multigroup multicast cellular and satellite communications: PHY layer design and link-level simulations," in *Proc. of the IEEE Intl. Conf. on Communications (ICC) Workshops*, 2021, pp. 1–6.
- [32] H. Cui, L. Zhu, Z. Xiao, B. Clerckx, and R. Zhang, "Energy-efficient rsma for multigroup multicast and multibeam satellite communications," *IEEE Wireless Commun. Lett.*, vol. 12, no. 5, pp. 838–842, May 2023.
- [33] H. Joudeh and B. Clerckx, "Sum-rate maximization for linearly precoded downlink multiuser MISO systems with partial CSIT: A rate-splitting approach," *IEEE Trans. Commun.*, vol. 64, no. 11, pp. 4847–4861, 2016.
- [34] S. S. Christensen, R. Agarwal, E. De Carvalho, and J. M. Cioffi, "Weighted sum-rate maximization using weighted mmse for mimo-bc beamforming design," *IEEE Trans. Wireless Commun.*, vol. 7, no. 12, pp. 4792–4799, Dec. 2008.
- [35] C. Mosquera and F. Gómez-Cuba, "Link Adaptation for Rate Splitting Systems with partial CSIT," *IEEE J. Sel. Areas Commun.*, vol. 41, no. 5, pp. 1336–1350, May 2023.
- [36] H. Minn, "A robust timing and frequency synchronization for OFDM systems," *IEEE Trans. Wireless Commun.*, vol. 2, no. 4, pp. 822–839, 2003.
- [37] P. Trifonov, "Efficient Design and Decoding of Polar Codes," *IEEE Trans. Commun.*, vol. 60, no. 11, pp. 3221–3227, 2012.
- [38] H. Li and J. Yuan, "A Practical Construction Method for Polar Codes in AWGN Channels," in *IEEE 2013 Tencon - Spring*, 2013, pp. 223–226.
- [39] I. Tal and A. Vardy, "List Decoding of Polar Codes," *IEEE Trans. Inf. Theory*, vol. 61, no. 5, pp. 2213–2226, 2015.